

# SYNTHESIS AND CHARACTERIZATION OF CHITOSAN BASED SILICA COMPOSITES DERIVED ASPARAGUS STALK END USED FOR REMOVAL OF CHROMIUM (VI) IONS FROM AQUEOUS SOLUTION\*

Aung Than Htwe<sup>1</sup>, May Thazin Kyaw<sup>2</sup>, Win Pa Pa Phy<sup>2</sup>, Moh Moh Zaw<sup>3</sup>,  
Cho Mar Kyi<sup>3</sup>, Theint Yee Mon<sup>3</sup>

## Abstract

The aim of the study was to prepare and characterize a chitosan based silica composite for the removal of Cr (VI) metal ions from aqueous solutions. In the current study, chitosan and silica were combined to prepare a chitosan-based silica composite with different mass ratios. Silica (SiO<sub>2</sub>) was obtained from the agricultural waste material of asparagus stalk ends. The prepared CS-SiO<sub>2</sub> composites were characterized by modern techniques like XRD, FT IR, SEM, UV-visible, and TG DTA analyses. The FT IR spectra showed the presence of new adsorption peaks (Si-O-Si bond), contributed by silica interaction with the hydroxyl group of chitosan. The study of morphology of the composite suggests that the SiO<sub>2</sub> particles were within the range of 2–7 nm in diameter and were uniformly dispersed in the polymer matrix. The thermal properties of these composite materials, indicated that the thermal stability of the chitosan was enhanced. Under the experimental conditions, which include pH of the solution, adsorbent dose, initial concentration, contact time the sorption properties of the CS-SiO<sub>2</sub> composite was observed for efficient removal of Cr (VI) ions from the aqueous solution. The adsorbent CS-SiO<sub>2</sub> composite showed a maximum removal percent of Cr (VI) ions of 94.65%. These findings suggested that silica obtained from asparagus stalk ends could be utilized to enhance chitosan characteristics, decrease agricultural waste dumping, and decrease Cr (VI) metal ions polluting water.

**Keywords:** chitosan, silica, CS-SiO<sub>2</sub> composite, Cr (VI) ions

## Introduction

Heavy metal pollution in wastewater is becoming severe with the rapid development of industry and has become a widespread concern worldwide (Liu *et al.*, 2022). Heavy metals such as mercury, cadmium, lead, chromium, and metal-like arsenic are of major environmental concern because they are non-biodegradable and cannot be decomposed or metabolized. Several metals cause serious health and environmental problems, and chromium (Cr) compounds are one of the most toxic contaminants in wastewater due to their high solubility, and toxicity, and free transferability (Du *et al.*, 2020).

Chromium contamination is a growing issue that frequently arises in industrial effluent from processes including metalworking, tanning leather, electroplating, and pigment production. Hexavalent chromium, Cr (VI) and trivalent chromium, Cr (III) are the two primary oxidation forms of chromium found in wastewater, and Cr (VI) is more hazardous to human health due to its greater carcinogenicity, teratogenicity, and mutagenicity.

Wastewater contains a variety of Cr (VI) species, including CrO<sub>4</sub><sup>2-</sup>, Cr<sub>2</sub>O<sub>7</sub><sup>2-</sup>, HCrO<sub>4</sub><sup>-</sup>, and H<sub>2</sub>CrO<sub>4</sub>. According to the World Health Organization (WHO), the maximum amount of

---

\* Second Prize (2023)

<sup>1</sup> Department of Chemistry, University of Yangon, Myanmar

<sup>2</sup> Department of Chemistry, University of Yangon, Myanmar

<sup>3</sup> Department of Chemistry, Mohnyin University, Myanmar

chromium that should be present in drinking water, is 0.05 mg/L. Therefore, it is necessary to develop effective methods to remove Cr (VI) from wastewater (Azizkhani *et al.*, 2020).

Adsorption processes can be performed through interactions between molecules of contaminants and adsorbents and mainly include hydrogen bonding, electrostatic bonding interactions, and  $\pi$ - $\pi$  interactions (Moradi *et al.*, 2021). Chitosan (CS) is a biopolymer derivative of chitin, a polysaccharide found abundantly in nature in crustacean exoskeletons of crab, shrimp, and lobster, as well as in the cuttlebone of cuttlefish. Chitosan has a lone pair of electrons on the amino and hydroxyl functional groups, which act as active sites for the removal of heavy metal ions from aqueous solutions (Mahatmanti *et al.* 2014).

SiO<sub>2</sub> particles are spherical in shapes and are of special importance due to their unique properties such as high active surface area, high mechanical and thermal resistance, non-toxicity, high porosity, dispersibility in different solvents, and environmental compatibility (Moradi *et al.*, 2021). Silica contains various silanol groups (Si-OH) on its outer shell, which act as suitable nucleation and anchor points for the natural functionalization of silica (Grace *et al.*, 2022). Thus, the silicon precursor shows quick in situ development of the silica network in the presence of ethanol and water via the sol-gel route, forming glassy, homogeneous, and transparent films compatible over a wide composition range (Sagheer and Muslim, 2009).

This research work focuses on the following key contributions: synthesis of chitosan-SiO<sub>2</sub> composites; characterization of chitosan-SiO<sub>2</sub> composites using SEM, FT IR, XRD, TG-DTA, and UV-visible analyses; and investigation of the adsorption capacity of Cr (VI) ions on CS-SiO<sub>2</sub> composites.

## Materials and Methods

Silica particles were prepared from asparagus stalk end and used after calcination at 500 °C for 4 hours. Chitosan was purchased from the British Drug House (BDH) Chemical England. All other chemicals used were of analytical reagent grade. In all investigations, the recommended standard methods and techniques involving both conventional and modern methods were provided.

### Preparation of Silica (SiO<sub>2</sub>) Derived Asparagus Stalk End Powder

Asparagus stalk end was collected, cleaned, dried and treated by thermal combustion under the controlled conditions at 500 °C for 4 h. The asparagus stalk end ash is treated with alkali extraction followed by acid treatment. The precipitate was washed several times with boiled distilled water to remove sulphate impurities and dried in a hot air oven. The powdered silica was refluxed with 1 M HCl at 80 °C for 2 h using the sand bath. Then it was dissolved in 1 M NaOH by continuous stirring for 2 h on a magnetic stirrer, and concentrated H<sub>2</sub>SO<sub>4</sub> was added drop by drop to adjust the pH in about 8. The precipitated silica was washed with warm water and after the washing process silica was dried at 60 °C for 6 h in the oven.

## Synthesis of Chitosan Based Silica Composite

Silica (0.1 to 0.5 g) was dissolved in each mixture of 30 mL of 1:2 (v/v) ethanol-water and 1 mL of 1M HCl solution and kept under constant stirring at 250 rpm for 30 min to obtain silica suspension. The suspended silica solution was added drop by drop into 100 mL of 1 % (w/v) chitosan solution (1g of chitosan in 100 mL of 1 % (v/v) acetic acid solution) and then was heated 60 °C at 100 rpm for 2 h. Then, 0.1 M NaOH was added dropwise to obtain gel and kept for 24 h. The precipitated CS-SiO<sub>2</sub> gel was centrifuged at 3000 rpm for 10 min and washed with distilled water to neutralize at pH 7. After that, the sample was dried in oven at 60 °C for 2 h and labeled as CS-SiO<sub>2</sub> (0.1g) (CSS 1), CS-SiO<sub>2</sub> (0.2 g) (CSS 2), CS-SiO<sub>2</sub> (0.3 g) (CSS 3), CS-SiO<sub>2</sub> (0.4 g) (CSS 4), and CS-SiO<sub>2</sub> (0.5 g) (CSS 5).

## Characterization of Chitosan Based Silica Composite

The prepared SiO<sub>2</sub> and CS-SiO<sub>2</sub> composites were analysed by FT IR spectrometer in a wide range of wavelengths between 400 cm<sup>-1</sup> and 4000 cm<sup>-1</sup> with a resolution of 1 cm<sup>-1</sup> and 3 scans/sample. The surface morphology of the prepared blend films were tested by JSM-5610 LV. Scanning Electron Microscope, JEOL at 20 kV. X-ray diffraction (XRD) analyses of prepared SiO<sub>2</sub> and CS-SiO<sub>2</sub> composites were carried out with Ni filtered Cu K $\alpha$  X-ray radiation. UV-visible spectra of the samples were collected from 185 to 600 nm using a UV-2550 spectrophotometer (Shimadzu) at room temperature. Thermogravimetric analysis was carried out in a nitrogen atmosphere at a heating rate of 15 °C/min up to a temperature of 1400 °C on the DTG-60H thermal analyzer.

## Batch adsorption experiments

The stock solution of Cr (VI) was prepared by dissolving acidified K<sub>2</sub>Cr<sub>2</sub>O<sub>7</sub> in deionized water. The solution concentrations required for the adsorption study were prepared by diluting this stock solution of Cr (VI). The pH of the prepared solutions was adjusted by using 0.1 M NaOH and 0.1 M HCl solutions. The effect of pH on the adsorption of Cr (VI) from aqueous solution on the adsorbents was investigated in different solution with a pH ranging from 3 to 7. The prepared CS, SiO<sub>2</sub>, CS-SiO<sub>2</sub> composites were added to Cr (VI) solution (50 ppm, 25 mL of Cr (VI), pH 5). The adsorbent doses from 0.1 to 0.5 g were investigated. After that, the impact of contact time in optimum conditions was studied by varying the contact time from 60 to 180 min. Adsorbent-adsorbate interaction was performed with a mechanic stirrer at 200 rpm for 1 h. After adsorption process, the amount of Cr (VI) remaining in the solution was determined with UV-visible spectrophotometer (Shimadzu UV2550) at 540 nm (Altun, 2020).

## Results and Discussion

### Preparation and Characterization of CS-SiO<sub>2</sub> Composites

Formation of silica on chitosan can occur through hydrogen bonds or van der Waals. Chitosan has many hydroxyl groups which can form hydrogen bonds with silanol groups as a result of hydrolysis. Another bonding mechanism between silica and chitosan by electrostatic attraction of chitosan undergoes protonation in an amino group and a hydroxyl group dissociating of silica in solution (Figure 1).

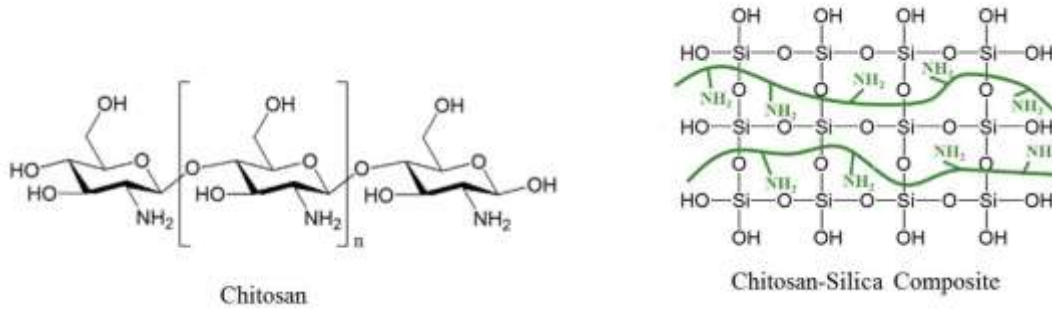


**Figure 1.** Chitosan and Chitosan-Silica Composite

### FT IR spectra analysis

FT IR analysis was carried out in the wavenumber range  $400\text{-}4000\text{ cm}^{-1}$ . FT IR spectra of  $\text{SiO}_2$ , CS, and CSS composite are displayed in Figure 2. Chitosan has a wide peak at  $3294\text{ cm}^{-1}$  (overlap between O-H and N-H groups). The peak at  $2880\text{ cm}^{-1}$  is C-H stretch, and amide groups can be observed at wavenumbers  $1656$ ,  $1583$  and  $1376\text{ cm}^{-1}$ . C-O stretch is also detected at  $1079\text{ cm}^{-1}$ . The characteristics  $\text{SiO}_2$  peak are the hydroxyl O-H of the silanol group and water that appears at wavenumbers  $3386$  and  $1638\text{ cm}^{-1}$ , Si-O groups at  $1095$ ,  $970$ ,  $802$  and  $466\text{ cm}^{-1}$  which show Si-O stretching, Si-OH stretching, Si-O stretching and Si-O-Si bending. The wavenumbers at  $1413$  and  $1423\text{ cm}^{-1}$  show the presence of C-H groups (asymmetric) on chitosan- $\text{SiO}_2$  composite and chitosan which are not present in  $\text{SiO}_2$ .

Figure 2 shows the FT IR spectra of the silica and silica-chitosan composite with  $\text{SiO}_2$  amount variations. A large vibration area peak at  $3424\text{ cm}^{-1}$  corresponds to O-H and N-H stretching. A small peak at  $1638\text{ cm}^{-1}$  relates to the possible interaction between the hydroxyl group of silica and the amine group of chitosan. Sharp peaks at  $1092\text{ cm}^{-1}$  and  $789\text{ cm}^{-1}$  are attributed to asymmetric and symmetric stretching vibration Si-O-Si. The peak at  $941\text{ cm}^{-1}$  indicates a functional group of Si-OH stretching vibration, and the peak at  $457\text{ cm}^{-1}$  indicates the existence of O-Si-O symmetric deformation vibration (Budnyak *et al.*, 2015).

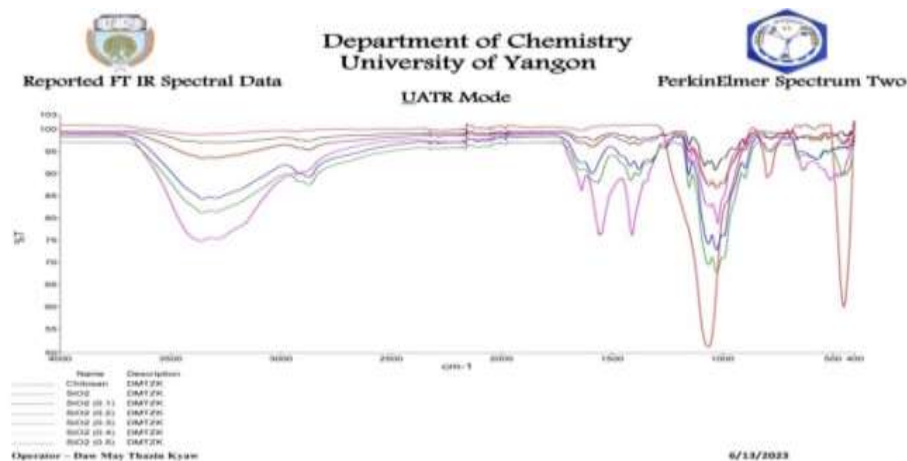


**Figure 2.** FT IR spectra of CS,  $\text{SiO}_2$  and CSS composites

### X-ray diffraction analysis

The XRD spectra of chitosan, SiO<sub>2</sub>, and chitosan-SiO<sub>2</sub> composites are shown in Figure 3. The diffraction peaks of CS exhibit two diffraction peaks at  $2\theta = 10^\circ$  and  $19.65^\circ$  which are the typical finger prints for chitosan powder. These two phases correspond to the hydrated crystallization and anhydrous crystallization of chitosan, respectively. The development of crystallinity in chitosan was due to the formation of hydrogen bonds between chains, and the crystalline form of chitosan changes with the conformation of chitosan (Siriprom *et al.*, 2018). The diffraction pattern of SiO<sub>2</sub> shows no polycrystalline peak except of the broad one centered at  $2\theta = 26.24^\circ$ , indicating that the SiO<sub>2</sub> has an amorphous-crystalline structure.

In the XRD patterns of CSS 1, CSS 2, CSS 3, CSS 4 and CSS 5, with the increase of silica content, the diffraction peak at  $2\theta = 10^\circ$  disappears, the intensity of the diffraction peak at  $2\theta = 20^\circ$  weakens and gradually shifts to  $2\theta = 23^\circ$ . The addition of silica will partially destroy the hydrogen bond between chitosan molecules and thus affect the crystal structure of chitosan. In addition, due to the presence of free amino groups and the spontaneous hydrophobic action of acids, chitosan is in an unstable state of loose double helices composed of polysaccharides asymmetric units, providing a large number of growth sites for amorphous silica formation (Zhong *et al.*, 2023).

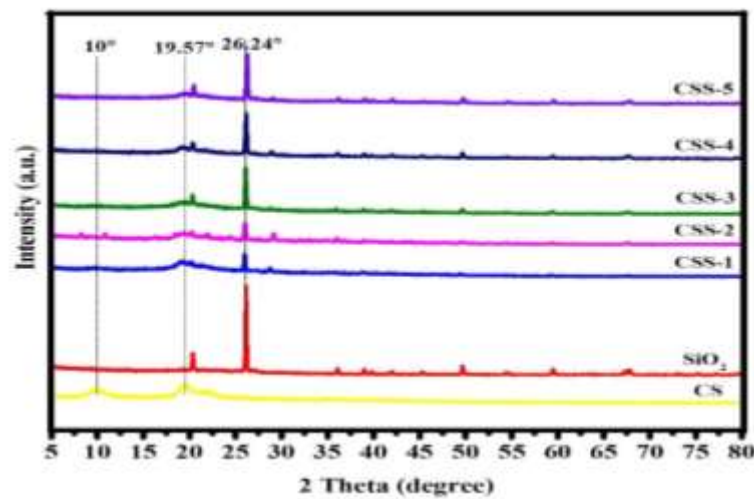


**Figure 3.** XRD patterns of CS, SiO<sub>2</sub> and CSS composites

### SEM Analysis

The morphology of CS, SiO<sub>2</sub>, CSS 1, CSS 2, CSS 3, CSS 4 and CSS 5 were observed with SEM images as shown in Figure 4. As can be seen from Figure 4(a), the surface fold of chitosan show a tight shape of polymeric fiber and accompanied by a few holes. SEM image of silica particles (Figure 4b) was distributed uniformly and tendency to arrange inhomogeneously. Silica nanoparticles are spherical in shape it is due to the even distribution during the process of composite preparation. From the SEM (Figures 4 c, d), CSS 1 and CSS 2 found many irregular spheres with obvious particles and holes. From the SEM (Figures 4 E, F) images of CSS 3 and CSS 4, it can be clearly seen porous coral-like micro/nano structure, and the pore size is in the nanometer range.

The SEM image of CSS 5 composite (Figure 4g) shows that SiO<sub>2</sub> is deposited tightly on the surface of chitosan, forming a uniform silica nanoparticle layer locally. In the precursor

solution, the alcohol hydroxyl group in chitosan can hydrogen-bond with  $\text{SiO}_2$ . However, with the increase of  $\text{SiO}_2$  content, excessive  $\text{SiO}_2$  will continue to hydrolyze and polycondense after encountering the residual strong acid on the surface of crystal nucleus, resulting in secondary growth of primary crystal nucleus and agglomeration of nanoparticles (Zhong *et al.*, 2023).

It can be concluded that the SEM image of all CSS composites showed that the composite was uniformly distributed and interaction between the silica and chitosan (Grace *et al.*, 2022).

To reveal the particle size distribution of the chitosan, silica and CS- $\text{SiO}_2$ , the particle images in Figures 4(a to g) were analyzed using Image J software. Figure 4(h) shows the particle size distribution of the CS,  $\text{SiO}_2$ , and all CSS composites. It can be seen that the silica and CS- $\text{SiO}_2$  tends to have a narrow particle size distribution than CS. It is also clearly noticed that the average diameter size distribution of silica is larger than that of CSS except CSS 5.

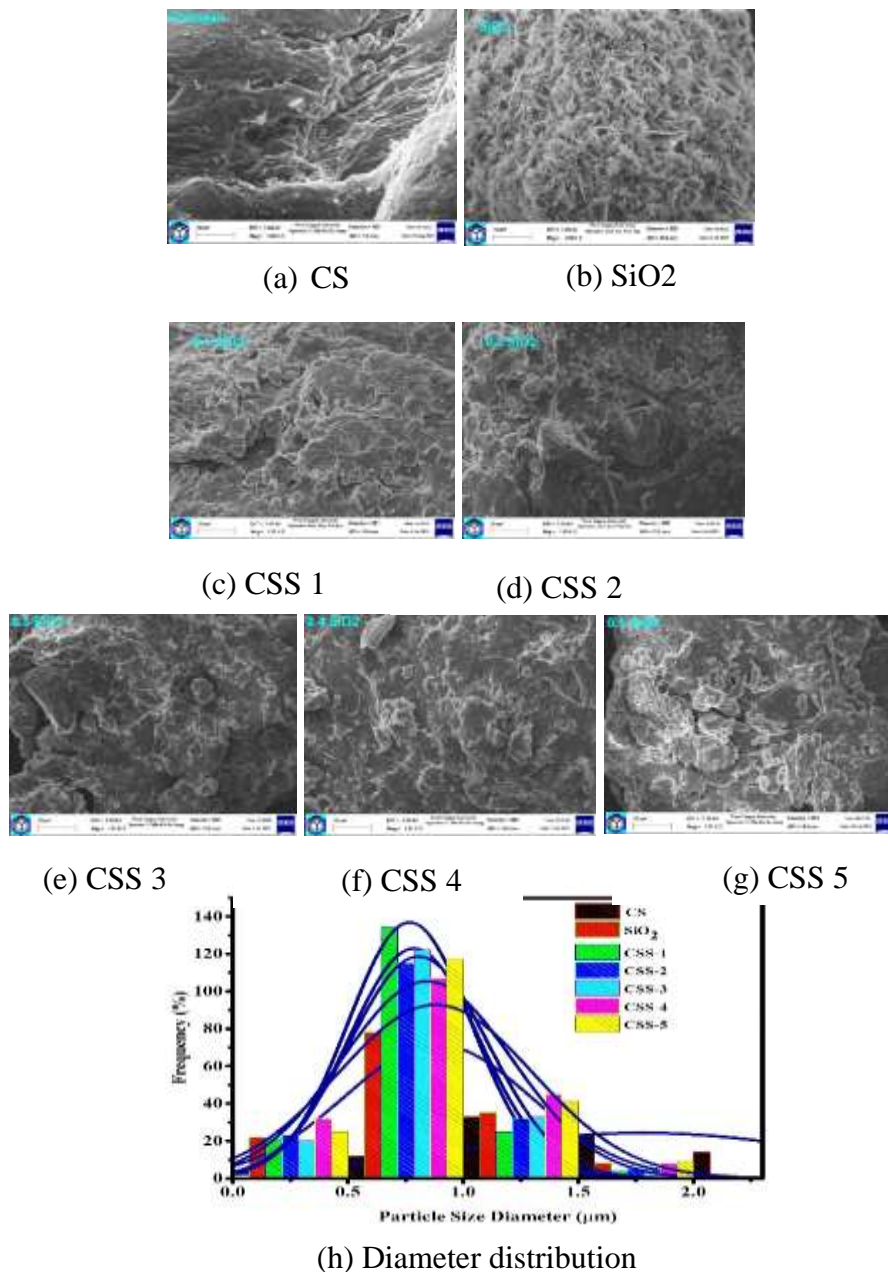


**Figure 4.** SEM images of (a) CS, (b)  $\text{SiO}_2$ , (c) to (g) CSS composites and (h) particle diameter size distribution

## Thermogravimetric analysis

Thermogravimetric analysis was performed to evaluate the thermal stability of materials as well as to confirm the amount of CS, SiO<sub>2</sub> and all prepared CS-SiO<sub>2</sub> composites. Thermograms of composites are shown in Figure 5(a) and DTA curves in Figure 5 (b). According to the TG thermogram profiles, CS showed three decomposition stages. The first stage has a temperature range of 38.86 °C to 252.52 °C and a weight loss of 14.70%. There is moisture evaporation upon heating. The second stage is the loss in weight 32.28 % was decomposed within the temperature range of 252.52 °C to 324.38 °C. This can be attributed to the weight loss peak of C-C single bond, C-O single bond and C-N single bond decomposition in chitosan. The third stage has a temperature range of 324.38 °C to 600 °C and a weight loss of 51.90 % with reference to the depolymerization and elimination of glycosidic units of CS, the decomposition at 100 °C is clearly observed. Thermal elimination of CS takes place above 200 °C after the residual water gets eliminated initially around 100 °C (Htwe *et al*, 2021). For SiO<sub>2</sub>, there is no obvious weight loss between 200 °C and 600 °C, the mass loss is only about 2.45 %, which can be attributed to the weight loss of Si-O-Si bond on the silica molecule.

The thermogram of all CSS shown in Figure 5(a), having a weight loss in three stage. The first weight loss (about 15 %) appeared at around 100 °C. There is caused by the evaporation of the trace amount of free and bound water contained in the sample due to physical absorption. In the second stage, a rapid weight loss (about 36 %) from the temperature range between 236 °C to 400 °C was observed. This can be attributed to the weight loss peak of C-C single bond, C-O single bond, C-N single bond decomposition in chitosan. When the dispersible SiO<sub>2</sub> nanoparticles form a composite material with chitosan, the intermolecular hydrogen bonding force in the chitosan chain is weakened, and the thermal decomposition temperature of chitosan chain degradation in the composite material is reduced (Zhong *et al.*, 2023). In third stage, a slow degradation from 400 °C to 600 °C representative of thermal degradation of deposited chitosan on the surface of the SiO<sub>2</sub> were observed with the weight loss of about 35 %. The significant increase in the weight residues at 600 °C illustrates successful incorporation of higher amounts of silica into the chitosan-SiO<sub>2</sub> and ultimately increases in thermal stability.

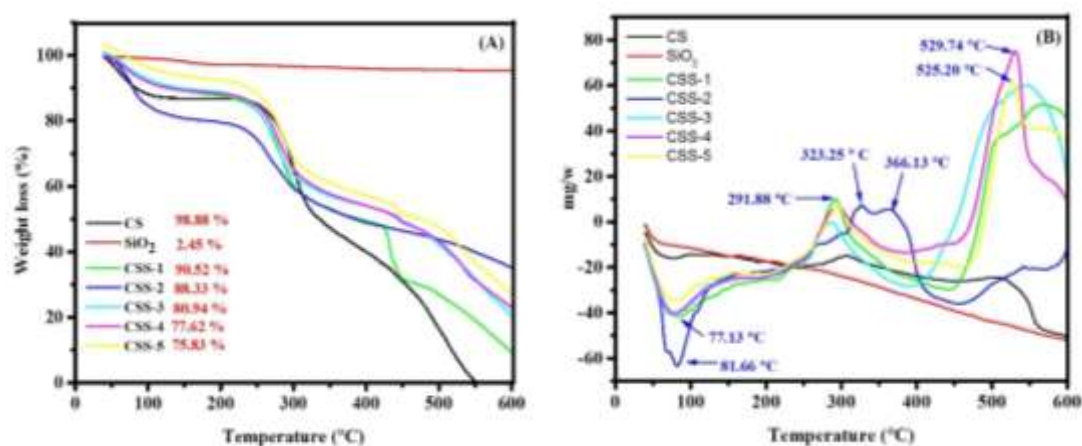


**Figure 5.** (a) TG curves and (b) DTA curves for CS, SiO<sub>2</sub> and CSS composites

## UV-visible absorption spectra

The UV-visible spectrum of chitosan, silica and chitosan silica composite are show in Figure 6 showed a single peak at around 200 nm. This single peak is characteristic of silica absorption spectrum and its intensity decreases with the decrease in the concentration of silica. The CS peaks shows at 239 nm and 289 nm. The CSS composite shows 289 nm, and 295 nm. It was found that the intensity of CSS composite is lower than that of CS and SiO<sub>2</sub>. Figure 6 shows the UV-visible absorption spectra of the suspension of naked and chitosan-coated SiO<sub>2</sub>. According to Figure 6(C to G), chitosan coating SiO<sub>2</sub> change in the UV-Vis spectra, and this confirms the binding of chitosan on SiO<sub>2</sub> nanoparticle.

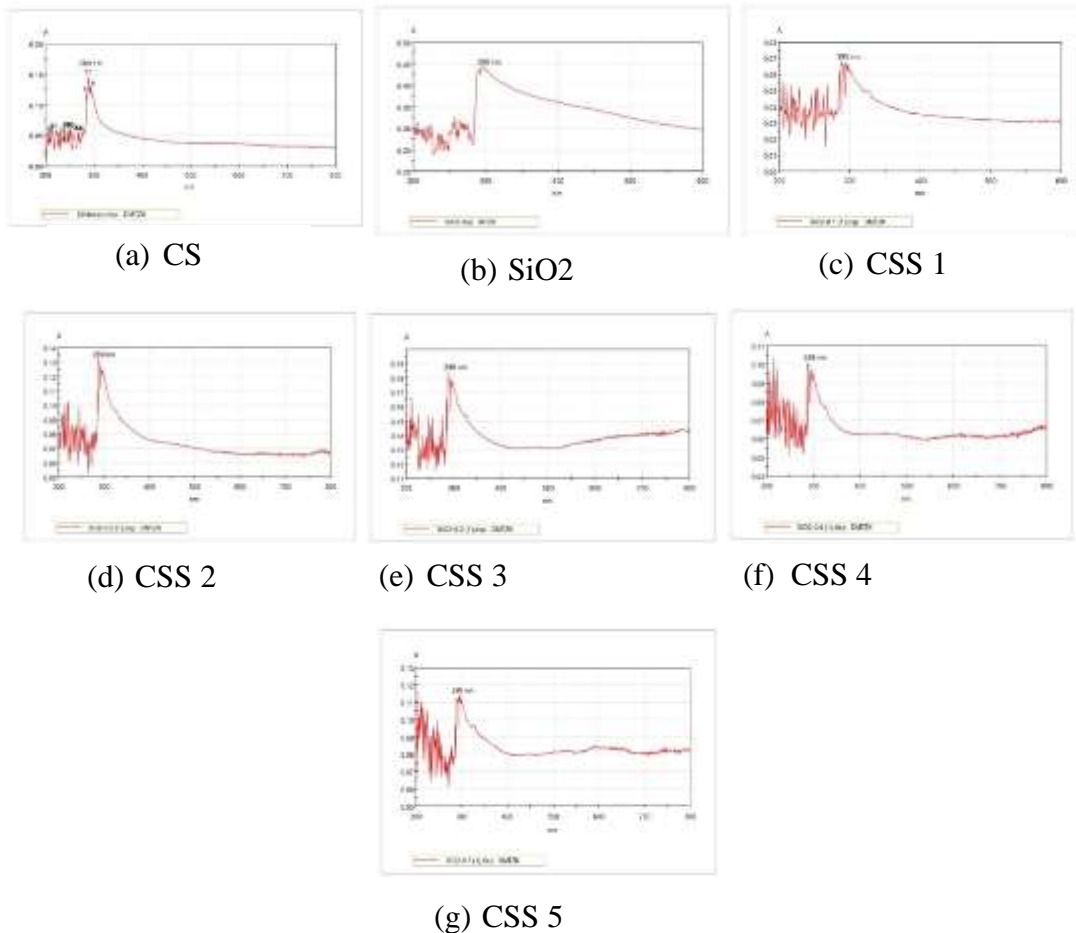


**Figure 6.** UV-Visible spectra of (a) CS, (b) SiO<sub>2</sub> and (c to g) CSS composites

## Adsorption performances of Cr (VI) ion with CS, SiO<sub>2</sub>, and CSS Composites

### Effect of pH

pH is one of the important parameters in the adsorption because it affects the surface mechanism of the adsorbent, in other words, to the binding points of pollutant and the adsorbent. The influence of initial pH on adsorption was studied in the range of 3-7 for initial metals ion concentration of 50 ppm by UV-visible spectrophotometer at 540 nm. As it can be seen in Figure 7, at pH 5, while 50 ppm Cr (VI) ion was removed with 79.18 % for SiO<sub>2</sub>, 82.98 % for CS, 87.39 % for CSS 1 and 90.89 % for CSS 5, this rate decreased to 28 % at pH 6. This situation can be attributed to the cationic structure of the adsorbent and to the presence of excess OH<sup>-</sup> ions in the solution. The maximum uptake of Cr (VI) ions took place at pH 4-5,

which may be attributable to the changes in the surface charge of the adsorbent. With an increase of the pH at above pH 5, the uptake of Cr (VI) ions decreased. The optimum pH of the Cr (VI) adsorption with the all composite adsorbent was found to be approximately 5. The species of Cr (VI) in aqueous solution were in the form of the bichromate ( $\text{HCrO}_4^-$ ), chromate ( $\text{CrO}_4^{2-}$ ) and dichromate ( $\text{Cr}_2\text{O}_7^{2-}$ ) ions. By increasing pH, decrease in adsorption percentage was observed. This might be due to the weakening of electrostatic force of attraction between the oppositely charged adsorbate and adsorbent that ultimately led to the reduction in sorption capacity (Baral *et al.*, 2006).

This may be attributed to the presence of free lone pair of electrons on nitrogen atoms of chitosan suitable for coordination with the metal ion to give the corresponding chitosan–metal complex (Donia *et al.*, 2008).

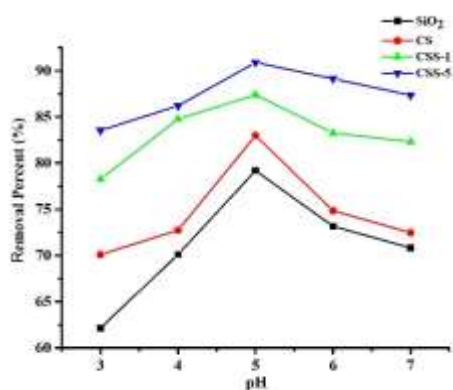


**Figure 7.** Effect of pH on adsorption of Cr (VI) ions onto CS, SiO<sub>2</sub> and CS-SiO<sub>2</sub> composites (condition: 0.4 g dosage /25 mL, 50 ppm of initial concentration, contact time - 120 min, 25 °C)

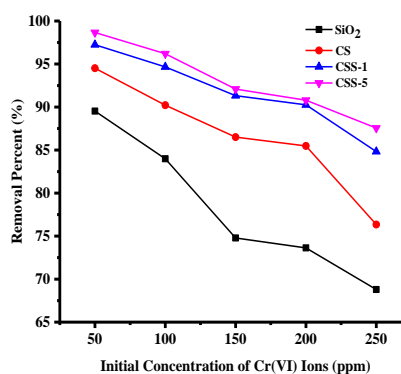


**Figure 8.** Effect of initial concentration of Cr (VI) ions onto CS, SiO<sub>2</sub> and CS-SiO<sub>2</sub> composites (condition: pH 5, 0.4 g dosage/ 25 mL, contact time - 120 min, 25 °C)

### Effect of initial metal ions concentration

The effect of initial concentration of Cr (VI) (50-250 ppm initial concentration range) on adsorption (initial solution pH 5, and adsorbent amount of 0.4 g/25 mL for SiO<sub>2</sub>, CS, CSS 1, and CSS 5 at 25°C) is shown in Figure 8. The results showed that the adsorption capacity decreased with the increase of initial Cr (VI) concentrations and therefore, decreased the removal percentage of Cr (VI) ions from 50 to 250 mg/L. It can be assumed that increasing initial metal concentration increases the number of collisions between Cr (VI) ions and adsorbents thus decreasing adsorption (Rahbar *et al.*, 2014). It can be concluded that the maximum removal of Cr (VI) ions (97 % by CSS 5) would occur for an initial concentration of 50 ppm.

### Effect of adsorbent dose

In terms of both the efficiency and cost of the process, it is of great importance to determine the appropriate adsorbent dosage in the adsorption processes. In this study, a series of experiments were performed with 50 ppm Cr (VI) solution in varying adsorbent dosages (0.1-0.5 g) and as a result, the effect of adsorbent amount on Cr (VI) adsorption was investigated. As seen

in Figure 9, it was observed that as the adsorbent dosage increased, the metal removal percent also increased. While Cr (VI) removal was 73.54 % for SiO<sub>2</sub>, 78.92 % for CS, 81.47 % for CSS 1 and 83.43 % for CSS 5 with 0.1 g adsorbent, it increased to 83.86 % for SiO<sub>2</sub>, 85.14 % for CS, 93.46 % for CSS 1 and 94.63 % for CSS 5 as the adsorbent dosage was increased to 0.4 g. Therefore, 0.4 g of adsorbent was regarded as the optimum dosage for the removal of Cr (VI) in this study. A higher dose provides a larger number of binding sites, which eventually causes the enhanced removal of Cr (VI). Increasing in adsorbent dose leads to increase in active sites of metal binding which means more metal ions are adsorbed. Hence, the adsorptivity increases till saturation. Any further addition of the adsorbent beyond 0.4 g did not cause any apparent change in the adsorptivity. The decrease in adsorption capacity can be attributed to the fact that some of the adsorption sites remain unsaturated during the adsorption process (Bandaru *et al.*, 2013).

### Effect of contact time

Contact time is one of the effective factors in the adsorption process. In this study, metal removal percentages were calculated in terms of contact time while all other parameters were kept constant. 0.4 g of adsorbent was mixed with 50 ppm Cr (VI) solution at pH 5 at varying time intervals and sorption percentage was drawn against contact time (Figure 10). From this investigation, adsorbed metal amount rapidly increased within a contact time of 30- 180 min, however, a significant difference was not observed for the measurements after 120 min. The effect of contact time on the adsorption of Cr (VI) were studied to determine the time taken by SiO<sub>2</sub>, CS, CSS 1, and CSS 5 composites to remove 50 ppm Cr (VI) solution at 25 °C. Figure 10 shows the adsorption capacity of SiO<sub>2</sub>, CS, CSS 1, and CSS 5 composites for Cr (VI) increased sharply within the first 90 min, which may be attributable to the availability of the sites on the surface of the adsorbent. It is suggested that a concentration gradient is present in both the adsorbent and adsorbate in the solution (Wu *et al.*, 2013). Then, it reached adsorption equilibrium at 120 min, and afterwards, there was no appreciable increase. Hence, the optimum contact time was taken to be 72 h for further studies. Hence, the optimal removal efficiency reached 97 % within about 120 min.

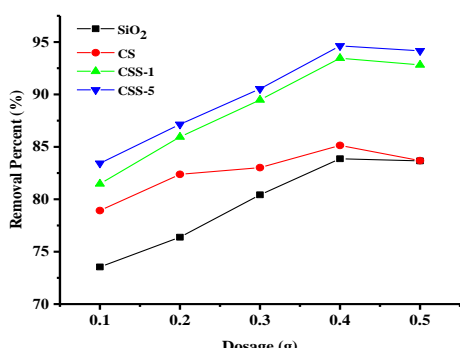


**Figure 9.** Effect of dosage of CS, SiO<sub>2</sub> and CSS composites on adsorption of Cr (VI) ions (condition: pH 5, 50 ppm of initial concentration, volume of 25 mL, contact time-120 min, 25 °C)

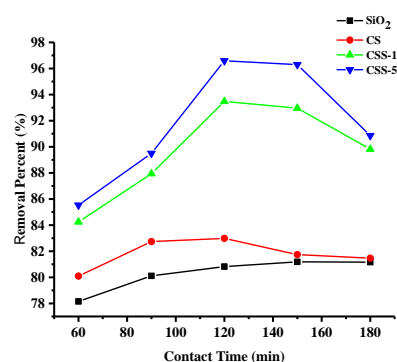


**Figure 10.** Effect of contact time on adsorption of Cr (VI) ions onto CS, SiO<sub>2</sub> and CSS composites (condition: pH 5, 50 ppm of initial concentration, 0.4 g dosage /25 mL, 25 °C)

In this study, the adsorption of heavy metal ion on chitosan based silica composite used as an adsorbent, which were derived from agricultural by-products, asparagus stalk end (silica). The CS-SiO<sub>2</sub> composite were prepared and characterized by FT IR, XRD, SEM, UV-visible and TG-DTA analyses. The results show that the morphology and properties of composites change with the introduction of silica. The CS-SiO<sub>2</sub> composite had a coral-like three-dimensional microporous, amorphous structure, and good thermal stability. The prepared CS-SiO<sub>2</sub> composites were used for the removal of Cr (VI) ions from an aqueous solution. The effect of several operating parameters, such as solution pH, initial Cr (VI) concentration, the dosage of adsorbents, and contact time, on the adsorption performance was examined by a batch system. When the dosage is 0.4 g/25 mL, the initial concentration of Cr (VI) ions solution is 50 mg/L, the pH of solution is 5, and the adsorption time is 120 min, the removal of Cr (VI) ions by CS-SiO<sub>2</sub> was observed 94.65 %.

The main contribution of the present work producing synthesis of chitosan based silica composite could promote to a certain extent of sustainable development goals and foster innovation engaging more on rural development toward and may be used for wastewater treatment.

### Acknowledgements

The author feel indebted to Professor and Head Dr Nyein Nyein Htwe, Department of Chemistry, Mohnyin University, Kachin State, Myanmar, for her stimulating suggestions.

### References

- Altun, T. (2020). "Preparation and Application of Glutaraldehyde Cross-Linked Chitosan Coated Bentonite Clay Capsules: Chromium(VI) Removal from Aqueous Solution". *J. Chil. Chem. Soc.*, vol. 65(2), pp. 4790-4797.
- Azizkhani, S., E. Mahmoudi, N. Abdullah, M.H.S. Ismail, A.W. Mohammad and S.A. Hussain. (2020). "Synthesis and Characterisation of Graphene Oxide-Silica-Chitosan for Eliminating the Pb(II) from Aqueous Solution". *Polymers*, vol. 12(1922), pp. 1-18.
- Bandaru, N.M., N. Reta, H. Dalal, A.V. Ellis, J. Shapter and N.H. Voelcker. (2013). "Enhanced Adsorption of Mercury Ions on Thiol Derivatized Single Wall Carbon Nanotubes". *Journal of Hazardous Materials*, vol. 261, pp. 534-541.
- Baral, S.S., S.N. Dasa and P. Rath. (2006). "Hexavalent Chromium Removal from Aqueous Solution by Adsorption on Treated Sawdust". *Biochem. Eng. J.*, vol. 31(3), pp. 216-222.
- Budnyak, T.M., I.V. Pylypchuk, V.A. Tertykh, E.S. Yanovska and D. Kolodynska. (2015). "Synthesis and Adsorption Properties of Chitosan-Silica Nanocomposite Prepared by Sol-Gel Method". *Nanoscale Research Letters*, vol. 10(87), pp. 1-10.
- Donia, A.M., A.A. Atia and K.Z. Elwakeel. (2008). "Selective Separation of Mercury(II) Using Magnetic Chitosan Resin Modified with Schiff's Base Derived from Thiourea and Glutaraldehyde". *J. Hazard. Mater.*, vol. 151, pp. 372-379.
- Du, X., C. Kishima, H. Zhang, N. Miyamoto and N. Kano. (2020). "Removal of Chromium(VI) by Chitosan Beads Modified with Sodium Dodecyl Sulfate (SDS)". *Appl. Sci.*, vol. 10(4745), pp. 1-23.
- Grace, A.S. and G.S.P.L. Malar. (2022). "Synthesis and Characterisation of Chitosan/Nanosilica Composite and Their Applications of Heavy Metal Ions Cu(II), Cr(II) and Pb(II) Removal from Aqueous Solution". *Tierärztliche Praxis*, vol. 42(3), pp. 95-107.

- Htwe, A.T., N.M. Tun, M.M. Soe, M. Gohdo, Y. Yoshida and N.N. Than. (2021). "Synthesis and Characterization of Chitosan Based Graphene Oxide Bionanocomposite". *J. Myanmar Acad. Arts Sci.*, vol. XIX(1B), pp. 213-226.
- Liu, Y., H. Shan, C. Zeng, H. Zhan and Y. Pang. (2022). "Removal of Cr(VI) from Wastewater Using Graphene Oxide-Chitosan Microspheres Modified with  $\alpha$ -FeO(OH)". *Materials*, vol. 15(4909), pp. 1-20.
- Mahatmanti, F.W., N. Nuryono and N. Narsito. (2014). "Physical Characteristics of Chitosan Based Film Modified with Silica and Polyethylene Glycol". *Indonesian Journal of Chemistry*, vol. 14(2), pp. 131-137.
- Moradi, O., S. Mhdavi, and S. Sedaghat. (2021). "Synthesis and Characterisation of Chitosan/Agar/SiO<sub>2</sub> Nano Hydrogels for Removal of Amoxicillin and of Naproxen from Pharmaceutical Contaminants". *Research Square*, pp. 1-23.
- Rahbar, N., A. Jahangiri, S. Boumi and M.J. Khodayar. (2014). "Mercury Removal from Aqueous Solutions with Chitosan-Coated Magnetite Nanoparticles Optimized Using the Box-Behnken Design". *Jundishapur J. Nat. Pharm. Prod.*, vol. 9(2), pp. 1-7.
- Sagheer, F.Al. and S. Muslim. (2010). "Thermal and Mechanical Properties of Chitosan/SiO<sub>2</sub> Hybrid Composites". *Journal of Nanomaterials*, vol. 2010, pp. 1-7
- Siriprom, W., K. Chantarasunthon and K. Teanchai. (2018). "Physical and Thermal Properties of Chitosan". In *Advanced Materials Research*, pp. 315-318
- Wu, Y., H.J. Wang, H. Wang, C. Zhang, J. Zhang and Z.L. Zhang. (2013). "Adsorption of Hexavalent Chromium from Aqueous Solutions by Graphene Modified with Cetytrimethylammonium Bromide". *J. Colloid Interface Sci.*, vol. 394, pp. 183-191
- Zhong, T., M. Xia, Z. Yao and C. Han. (2023). "Chitosan/Silica Nanocomposite Preparation from Shrimp Shell and Its Adsorption Performance for Methylene Blue". *Sustainability*, vol. 15(47), pp. 1-19